

TRIPLE S: A NEW TOOL FOR SOYBEAN HIGH THROUGHPUT PHENOTYPING FROM UAS-BASED MULTISPECTRAL IMAGERY

Monica Herrero-Huerta ^{a, *}, Saravanan Govindarajan ^b, Keith A. Cherkauer ^c and Katy M. Rainey^a

^a Department of Agronomy, Purdue University, West Lafayette, Indiana (USA);

^b Electronics and Communications Engineering, Vellore Institute of Technology, Chennai, India;

^c Agricultural and Biological Engineering, Purdue University, West Lafayette, Indiana (USA)

* Corresponding author: mherrero@purdue.edu

ABSTRACT

Precise and functional phenotyping is a limiting factor for crop genetic improvement. However, because of its ease of application, imagery-based phenomics represents the next breakthrough for improving the rates of genetic gains in field crops. Currently, crop breeders lack the know-how and computational tools to include such traits in breeding pipelines. A fully automatic user-friendly data management together with a more powerful and accurate interpretation of results should increase the use of field high throughput phenotyping platforms (HTPPs) and, therefore, increasing the efficiency of crop genetic improvement to meet the needs of future generations.

The aim of this study is to generate a methodology to high throughput phenotyping based on temporal multispectral imagery (MSI) collected from Unmanned Aerial Systems (UAS) in soybean crops. In this context, ‘Triple S’ (Statistical computing of Segmented Soybean multispectral imagery) is developed as an open-source software tool to statistically analyze the pixel values of soybean end-member and to compute canopy cover area, number and length of soybean rows from georeferenced multispectral images. During the growing season of 2017, a soybean experiment was carried out at the Agronomy Center for Research and Education (ACRE) in West-Lafayette (Indiana, USA). Periodic images were acquired by Parrot Sequoia Multispectral sensor on board senseFly eBee.

The results confirm the feasibility of the proposed methodology, providing scalability to a comprehensive analysis of crop extension and affording a constant operational improvement and proactive management.

Key words: Remote Sensing, Unmanned Aerial System (UAS), Multispectral Imagery, High-Throughput Phenotyping, Soybean, Triple S.

1. INTRODUCTION

Recent advances in sensor technology, Unmanned Aerial Systems (UASs) and computing processes promote exponential growth in remote sensing applications. Regarding the acquisition platform, equipped with multiple imaging sensors, autopilots and GNSS / IMU (Global Navigation Satellite System / Inertial Measurement Unit), UASs have become one of the most viable remote sensing tools offering great possibilities for precision agriculture [1] and high-throughput phenotyping [2]. One of these breakthrough is automated high-throughput crop phenotyping using low-cost aerial images for estimating biophysical and biochemical plant parameters [3], capable to assist in decision making for genetic inference and selection of phenotypes of extensive crop areas. Computer vision systems are highly suitable for this purpose because they are a non-contact and non-destructive technique [4]. The application scenarios of digital image analysis and 3D modelling cover yield estimation, quality evaluation, disease detection and phenology [5].

Various agronomic parameters and phenotypic traits have been reported in previous studies based on the sensors on board UASs. For instance, low-cost multispectral sensors in VIS and Near Infrared (NIR) allow extraction of both physiological and geometric properties of vegetation [6] as well as accurate estimation of chlorophyll content, N concentration and yield for a variety of crops [7]. The explanation is clear: the spectral signature of a given crop is directly related to its phenological,

physiological and morphological characteristics, such that any change in the plant will also disturb its reflectance [8]. These differences in the intrinsic spectral behaviour of each species allow their discrimination and mapping by analysis techniques and digital classification. Moreover, RGB images were used to accurately estimate vegetation index by deep neural network [9]. In addition, thermal sensors provide plant canopy temperature, which has been used to detect water stress [10]. Concretely, in row crops, such as corn and soybean, canopy temperature during seed fill is an important indicator of crop health and yield potential.

In this research, a fully automatic photogrammetric pipeline is used to process the data via two main steps: first, the automatic determination of the view of each image; second, the automatic computation of the 3D coordinates for the generation of a dense and scaled 3D model of the scene and the subsequently orthomosaic. Subsequently, vegetation index mapping is computed in order to show the potential of multispectral calibrated images in agronomy. After that, ‘Triple S’ (Statistical computing of Segmented Soybean multispectral imagery) is applied to statistically analysis the pixel values of soybean end-member by filtering the image through k-means clustering. Moreover, canopy cover area, number and length of soybean rows is calculated by extracting the edge map via canny algorithm and using PCA (Principal Component Analysis).

The paper is organized as follow: after this brief introduction, the employed materials and the proposed methodology are described. Subsequently, the results with a proper discussion are presented. To finalize, an outlook pointing out the conclusions is summarized.

2. MATERIALS

The employed equipment for the data acquisition is described:

- A GNSS device from TopCon to georeference the Ground Control Points (GCP).
- A general purpose GER 1500 spectroradiometer to acquire spectral measurements of the calibration targets. The main technical specifications are described in Table 1.

Table 1. Technical specifications of the GER 1500 Spectroradiometer.

Parameter	Value
Spectral range	350-1050 nm
Spectral Channels	512
Spectral resolution	1.5 nm
Field of view	4° std
Shooting time	1 s

- A four narrowband passive sensor: Parrot Sequoia Multispectral sensor. The camera specifications and filters are detailed in Table 2 and 3. It has a global shutter to avoid problems in data processing [11] and it is self-calibrate by using the incorporated Sunshine sensor.

Table 2. Technical specifications of the Parrot Sequoia Multispectral sensor.

Parameter	Value
Spectral range	350-2500 nm
Shooting time	0.1 s
Spectral resolution	1 nm
Field of view	25°

Table 3. Channel specifications of the narrowband Parrot Sequoia Multispectral sensor.

Channel	Band	λ_{mean} [nm]	Bandwidth [nm]
1	Green	550	40
2	Red	660	40
3	Red-edge	735	10
4	Near infrared	790	40

- The senseFly eBee, designed as a fixed wing UAV for application in precision agriculture with incorporated GPS, IMU and magnetometer. It has a weight of 700 g and a payload of 150 g. Parrot Sequoia Multispectral sensor is controlled by the senseFly eBee autopilot during the flight.

3. METHODOLOGY

The proposed workflow is illustrated in Figure 1. As inputs from the soybean breeding field, multispectral images from UAS have to be acquired at the same time as spectral field measurements over reflectance targets to robustly check the reflectance values. Moreover, a survey campaign of GCP was done to properly geo-reference the images. Then, the processing starts with a low-cost photogrammetric pipeline to get the VI mapping of the plots. Coming up next, Triple S software is run over the data plot, computing statistical parameters of the segmented soybean, canopy cover and number and length of each row. This process will allow to the breeders to analyze the genetic inference and phenotyping selection of soybean.

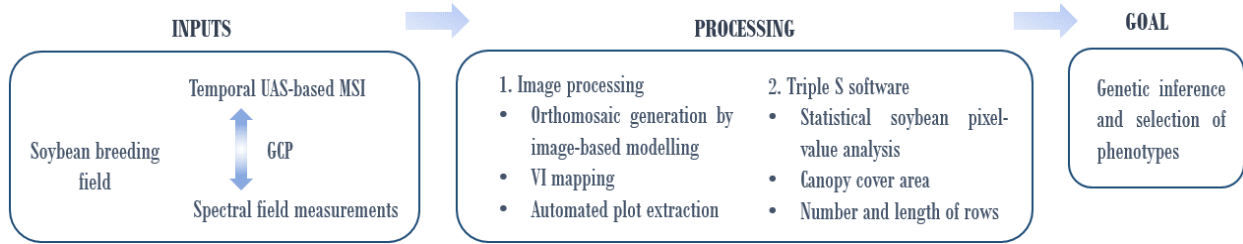


Figure 1. Workflow of the proposed methodology.

3.1. Image processing

In an attempt to guarantee automation and quality in the image processing, a combination of photogrammetric and computer vision techniques is required. Thereby, multispectral dataset are treated using a pipeline based on camera calibration [12], image orientation (bundle adjustment), dense point cloud extraction [13] and orthophoto production [14]. The Pix4Dmapper software package (Pix4D SA, Lausanne, Switzerland) is used for image processing. Moreover, a topographic survey campaign is established to obtain absolute georeferencing and a model scaled through GCPs. These observations are used as well in retrieving the camera interior parameters and correcting for any systematic error or block deformation. The Parrot Sequoia Multispectral sensor is a self-calibrating system. It incorporates an integrated irradiance sensor that allows irradiance values synchronized to the onboard GPS, IMU and magnetometer. The relative influence of the atmosphere is minimal because the atmospheric column spanned by the radiation is unimportant and can be neglected in the calculations [15]. To finalize, generated orthomosaics for each band are accurately geo-referenced to EPSG 32616, WGS84 CRS and the bands are merged, taking into account the parallax, using the Geospatial Data Abstraction Library (GDAL).

Next step is to compute different vegetation index mapping. These images were processed with algorithms defined in the Red and Near Infra-Red bands and their normalization of soil background brightness through an implemented code in GNU Octave software.

In order to get useful information about each plot in the field, we need to extract plot level data from the orthomosaic VI image. Individual plot boundaries need to be extracted and defined separately from images with an assigned plot ID that defines their genomic type by a field-map based plot extraction. In this approach, first we created a KML file from the field map using QGIS open source software. The script starts from the top right and builds the first polygon using the defined plot size and skips the gap between plots and generates the next one until it gets to the last plot on the bottom left. One advantage is that it can be generalized to other crop types as long as the field map is provided and the plots are planted in regular distance and have a consistent size within a trial.

3.2. ‘Triple S’ software (Statistical computing of Segmented Soybean multispectral imagery)

Once the individual plots are extracted, ‘Triple S’ software (Statistical computing of Segmented Soybean multispectral imagery) is running. ‘Triple S’ is an open tool coded in Python and uses GDAL library and Open Source Computer Vision Library [16] running over Anaconda Prompt. From each plot, it generates the following information ordered in an excel sheet by the name of the plot file:

- i. Firstly, the image is classified in ground and soybean by k -means clustering [17] using the near infrared band, which provides a bigger difference of the spectral response between end-members. The algorithm assigns a cluster (k clusters) to each pixel ($x_{i,i}=1..n$). K -means is a clustering method that aims to find the positions $\mu_{i,i}=1..k$ of the clusters that minimize the radiance variance (r) from the pixels to the cluster (Equation 1):

$$\arg \min_c \sum_{i=1}^k \sum_{x \in c_i} d(x, \mu_i) = \arg \min_c \sum_{i=1}^k \sum_{x \in c_i} \|x - \mu_i\|_2^2 \quad (1)$$

where c_i is the set of pixels that belong to cluster i .

Once the image is filtered, the statistical parameters of the pixel-values of soybean end-member are calculated (mean, medium and standard deviation).

- ii. In the second step, canopy cover area (m^2) is obtained by reading the coordinates in the metadata and relating to the number of soybean end-member pixels.
- iii. The next step consists on acquiring the number of rows through an edge map that define if the row is completed. Canny algorithm [18] is used to obtain the edge map from the NIR band, in this case. Canny algorithm is a widely used edge detection method. It is a multi-step algorithm that consists on smoothing of the image using a Gaussian Filter to remove the noise, computing the intensity gradients of the image, double thresholding the image to get potential edges and deleting all edges that are not connected to a strong edge. When the edge map is computed, left and right side of the row is defined by the orientation.
- iv. Finally yet importantly, Principal Component Analysis (PCA) is used [19] to compute the length of each row. This statistical analysis uses the first and second moments of the soybean pixels from the same row and results in two orthogonal vectors centered on the center of gravity of the row. PCA synthesizes the distribution of pixels along the two dimensions and therefore models the principal directions and magnitudes of variation of the pixel distribution around the center of gravity. The coordinates x_i and y_i for each pixels $i=1, \dots, k$ from the image of each row is considered. The covariance matrix (Σ) (2) of each row (X) is defined by:

$$\Sigma = \frac{(X-\bar{X})^T (X-\bar{X})}{k} = \begin{pmatrix} \sigma_x^2 & \sigma_{xy} \\ \sigma_{xy} & \sigma_y^2 \end{pmatrix} \quad (2)$$

where (σ_x^2, σ_y^2) are the variances of the pixel directions and the elements outside the main diagonal of Σ are the covariances. \bar{X} contains k copies of the mean of the two coordinates of the row pixels (X). The row length is the number of soybean pixels along the first eigenvector of Σ [20].

4. EXPERIMENTAL RESULTS AND DISCUSSION

The soybean experiment was carried out at the Agronomy Center for Research and Education (ACRE) during 2017 growing season in West-Lafayette (Indiana, USA). Figure 2 locates the study area with an image from RGB UAV data. The study area has an extension of $252.4 \times 109.5 \text{ m}^2$, consisting of 20 plots in vertical and 48 plots in horizontal, with different sizes depending of the number of horizontal rows with the same genotype (4, 8 and 6 rows). The photogrammetric flight configuration was with along-and across-track overlap of ca. 75%, adequate to Pix4D software processing. A flight altitude over the ground of 79 m is obtained by Sensefly software, given the camera focal and the required Ground Sample Distance (GSD). GCPs were placed on the ground for scaling, georeferencing and analysis purposes and measured with GNSS.

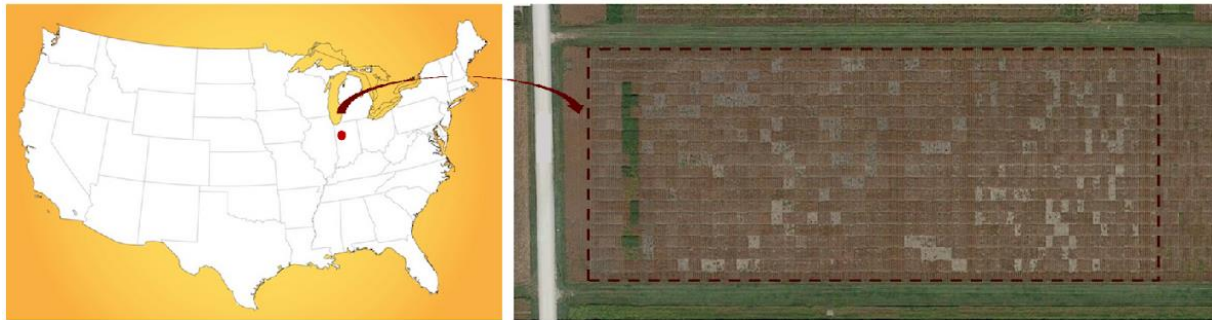


Figure 2. Location of the study area of soyben crop in West-Lafayette (Indiana, USA) (left) with a detailed zoom from RGB UAV data (right).

Images captured by the Parrot Sequoia Multispectral sensor generate datasets for each flight that included Green, Red, Red Edge and NIR information. The analysis of data captured by multispectral cameras requires prior knowledge of the radiometric calibration parameters of each channel to obtain correct interpretations [15]. For this reason, at the same time to the aerial data acquisition, a radiometric campaign on field was carried out to radiometrically check the calibration of the sensor. Thus, calibration targets were placed in the study area and measured by the spectroradiometer.

Periodic images were acquired by Parrot Sequoia Multispectral sensor on board senseFly eBee, which provides a great flexibility to quickly perform vegetation index mapping in high spatial, temporal and spectral resolution. The weather conditions on these days were clear and free cloud during noon time, when the flights were done. Data is separately processed per band by a photogrammetric pipeline using Pix4D to obtain the orthomosaic required for GIS integration. After that, georeferenced index vegetation mapping is performed based on calculation between different bands taking into account the parallax and the GCPs. Figure 3 illustrates VI mapping over the study area on July 26, 2017: the Normalized Difference Vegetation Index (NDVI) (a), the Soil Adjusted Vegetation Index (SAVI) (b), the Modified Soil Adjusted Vegetation Index (MSAVI) (c) and the Generalized Soil Adjusted Vegetation Index (GESAVI) (d). Although the indices addressed here do not have the same range of variation, all of them identify the plant trellis in the scene. The darkest plots correspond to non-vegetated areas because the plants did not grown.

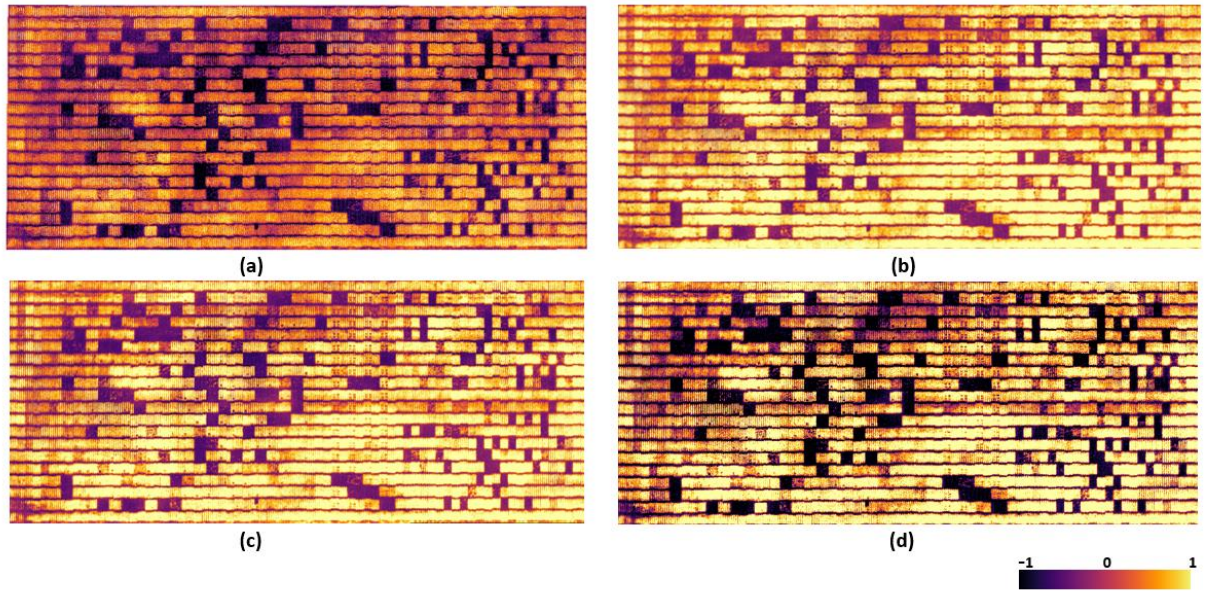


Figure 3. VI mapping on July 26th, 2017 over the study area (DL (499919.5, 4481053.9); UR (500171.9, 4481163.4); EPSG 32616): NDVI (a), SAVI (b), MSAVI (c) and GESAVI (d).

To accurately reflect the actual breeding field planting configuration, a script is developed to overlay defined plot sizes with known spacing and eliminating border effect by changing the plot size. This automated plot extraction allows us to analyze each breeding plot. Figure 4 illustrates randomly selected plots after the extraction over the study area, consisting of 960 individual plots with variable size.

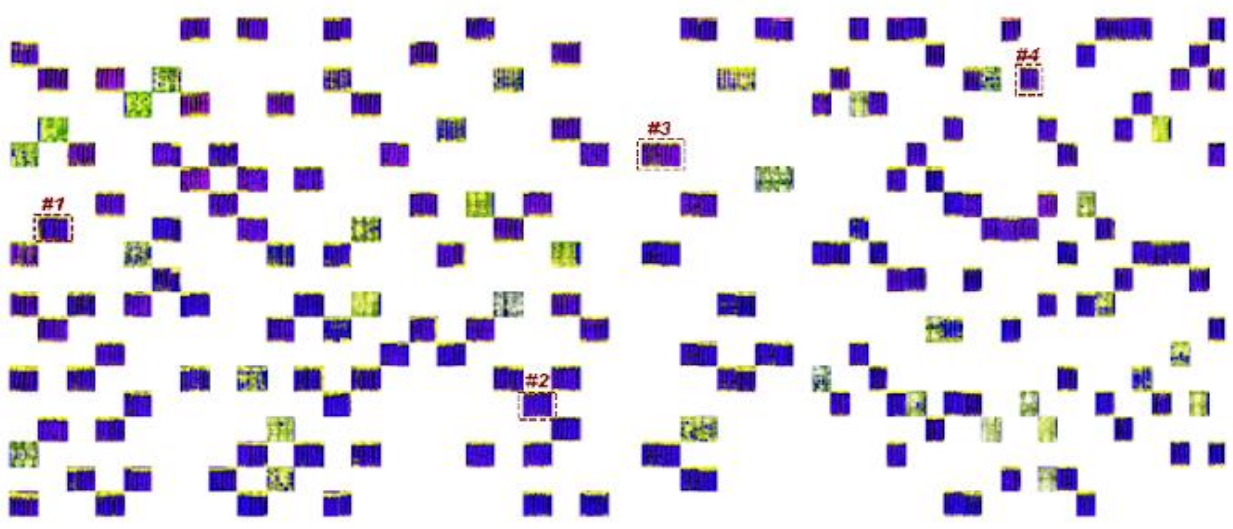


Figure 4. Randomly selected plots from the study area (DL (499919.5, 4481053.9); UR (500171.9, 448116.3); EPSG 32616) and the 4 particular plots for a deeper analysis.

For each plots, Triple S software is run. 4 plots are selected to present the results, marked in Figure 4, at 4 different phenological stages depending on the epoch from the 2017 planting date (May 31st, 2017) to show the results. These selected plots correspond to different seed breeding genetics. The image acquisition dates are June 27th, July 14th and 26th and August 18th, 2017. Below, the results per band from Triple S of the 4 particular plots at the 4 selected dates are summarized in Table 4: mean (\bar{x}_i), median (med_i) and standard deviation (σ_{xi}) value of soybean end-member reflectance and unsupervised classification threshold computed for NIR band (band 4).

Table 4. Results per band from Triple S of the 4 particular plots at selected dates: mean (\bar{x}_i), median (med_i) and standard deviation (σ_{xi}) value of soybean end-member reflectance and classification threshold computed for NIR band (band 4).

Plot	Date (MM/DD)	\bar{x}_1	\bar{x}_2	\bar{x}_3	\bar{x}_4	med_1	med_2	med_3	med_4	σ_{x1}	σ_{x2}	σ_{x3}	σ_{x4}	Thr.
1	06/27	0.0748	0.0715	0.1910	0.2198	0.0737	0.0716	0.1837	0.2240	0.0091	0.0160	0.0158	0.0181	0.200
	07/14	0.0590	0.0355	0.2455	0.3608	0.0615	0.0369	0.2409	0.3599	0.0068	0.0525	0.0768	0.0768	0.200
	07/26	0.0410	0.0214	0.2522	0.3560	0.0360	0.0215	0.2307	0.3495	0.0054	0.0082	0.0322	0.0527	0.230
	08/18	0.0412	0.0300	0.3176	0.6315	0.0357	0.0298	0.3177	0.6300	0.0042	0.0050	0.0817	0.0816	0.390
2	06/27	0.0905	0.0967	0.2130	0.2506	0.0896	0.0924	0.2085	0.2501	0.0137	0.0271	0.0164	0.0188	0.230
	07/14	0.0680	0.0379	0.3032	0.4012	0.0570	0.0319	0.2725	0.4005	0.0068	0.0075	0.0546	0.0822	0.215
	07/26	0.0398	0.0254	0.2632	0.4232	0.0429	0.0230	0.2631	0.4183	0.0055	0.0063	0.0277	0.0429	0.315
	08/18	0.0555	0.0298	0.3189	0.6646	0.0411	0.0312	0.3188	0.6645	0.0069	0.0167	0.0499	0.0992	0.315
3	06/27	0.0813	0.0712	0.1802	0.2198	0.0786	0.0734	0.1796	0.2219	0.0066	0.0131	0.0160	0.0204	0.195
	07/14	0.0688	0.0369	0.2422	0.3809	0.0619	0.0332	0.2524	0.3806	0.0072	0.0033	0.0564	0.0725	0.225
	07/26	0.0420	0.0211	0.2766	0.4156	0.0480	0.0241	0.2780	0.4186	0.0052	0.0050	0.0293	0.0444	0.315
	08/18	0.0311	0.0310	0.3541	0.6121	0.0373	0.0311	0.3555	0.6155	0.0046	0.0047	0.0671	0.0470	0.515
4	06/27	0.0850	0.0820	0.2003	0.2401	0.0790	0.0741	0.1958	0.2396	0.0087	0.0179	0.0123	0.0170	0.215
	07/14	0.0572	0.0366	0.2625	0.3901	0.0598	0.0342	0.2727	0.3838	0.0056	0.0024	0.0481	0.0552	0.265
	07/26	0.0437	0.0242	0.2900	0.3952	0.0439	0.0244	0.2541	0.3892	0.0044	0.0045	0.0213	0.0332	0.315
	08/18	0.0411	0.0311	0.3323	0.5751	0.0374	0.0334	0.3324	0.5746	0.0051	0.0063	0.0597	0.0451	0.450

As an analysis, we can see how the outliers influence the values, making a large difference between mean and median value but being NIR band (band 4) the most consistent band for vegetal response as expected. The standard deviation represents the spatial variability in reflectance with no correlation found along time per band. The threshold is the value obtained using *K-means* to mask the soybean member using NIR band (band 4).

In Table 5, number of pixels, number and length average of detected rows and Canopy Cover per image is summarized. Canopy cover is increasing along the time for all plots, same as the row length, where the growing evolution is exemplified. It is worth to mention that some holes along the rows are detected and quantified.

Table 5. Results from Triple S of the 4 particular plots at selected dates: number of pixels and rows and row length and Canopy Cover per plot.

Plot	Date (MM/DD)	No. pixels	No. rows	Lmean (m)	CC (m ²)
1	06/27			3.92	3.69
	07/14	6320	6	4.03	11.54
	07/26			4.19	12.13
	08/18			4.16	20.16
2	06/27			3.98	4.59
	07/14	6320	6	4.09	12.00
	07/26			4.11	13.22
	08/18			4.18	21.45
3	06/27			4.04	5.10
	07/14	8374	8	3.96	14.51
	07/26			3.99	14.03
	08/18			4.18	19.00
4	06/27			4.01	2.36
	07/14	4187	4	4.06	6.83
	07/26			4.11	7.71
	08/18			4.14	13.25

Figure 5 shows how plot 3 is evolving for selected dates (June 27th, July 14th and 26th and August 18th, 2017) using Triple S regarding the edge map and canopy cover computation and quantified.

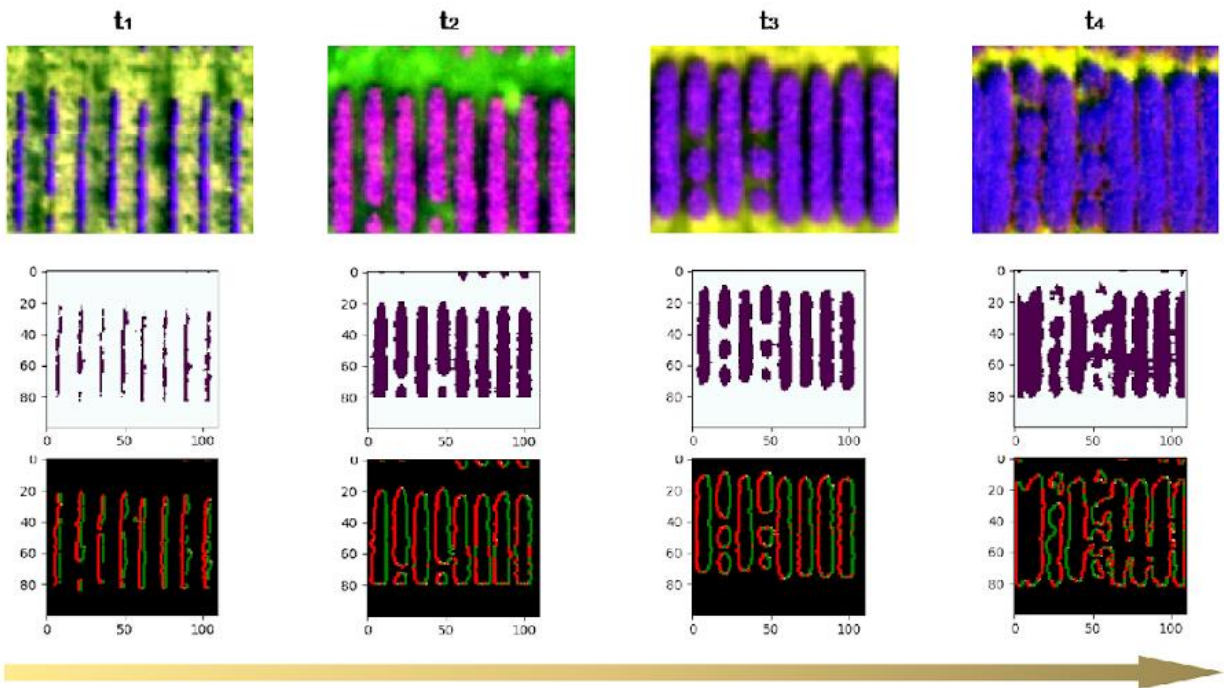


Figure 5. Plot 3 evolution for selected dates (June 27th, July 14th and 26th and August 18th, 2017) using Triple S software to compute the edge map.

In particular, we compare the 4th plots at July 26th, 2017, to check which plot formed by different genomics generated more biomass. Therefore, we use the median reflectance per band to calculate the vegetation index value per plot related to the mean productivity and biomass [21]. In Table 6, different vegetation indexes are obtained by the mean reflectance values through ‘Triple S’ in the selected times and plots. The mean value classifications for all indexes confirms that plot #2 has a higher biomass production, with a NDVI increment of 8% and 20% in GSAVI index regarding the average value from all the plots. From a temporal study, plot #4 shows a better development from July 14th to 26th, with a SAVI increment of 23% and a NDVI increment of 24%.

Table 6. Vegetation index values from different plots along the time.

Plot	Date (MM/DD)	NDVI	SAVI	MSAVI	GSAVI
# 1	27-Jun	0.10	0.07	0.48	-0.01
	14-Jul	0.20	0.16	0.76	0.11
	26-Jul	0.20	0.16	0.78	0.11
	18-Aug	0.33	0.32	0.81	0.36

	27-Jun	0.09	0.07	0.44	-0.01
# 2	14-Jul	0.19	0.16	0.71	0.11
	26-Jul	0.23	0.20	0.81	0.16
	18-Aug	0.35	0.35	0.80	0.41
	27-Jun	0.11	0.07	0.50	0.00
# 3	14-Jul	0.20	0.17	0.76	0.12
	26-Jul	0.20	0.18	0.73	0.13
	18-Aug	0.27	0.27	0.67	0.26
	27-Jun	0.10	0.07	0.48	-0.01
# 4	14-Jul	0.17	0.14	0.65	0.08
	26-Jul	0.21	0.18	0.78	0.13
	18-Aug	0.27	0.26	0.73	0.25

After this analysis, we can assure that high temporal and spatial resolution multispectral images from UAS allow crops to be monitored for diseases or managing water supply and nutrients, as well as decisions to be made about phenotyping selection.

5. OUTLOOK

This paper proves the great potential of UAS to collect multispectral images for soybean phenotyping as a fast, reliable and economic resource. Moreover, the proposed framework demonstrates that it is highly feasible to provide relatively accurate estimation of plant traits and provide valuable insight for high spatial precision in agriculture, plant stress assessment, genetic inference and phenotyping selection. It is worth mentioned that this workflow can be effectively employed for other HTPPs and crops planted in breeding nurseries.

Nevertheless, the UAS approach for precision farming is in constant evolution and represents an extremely dynamic sector. In this context, Triple S software (Statistical computing of Segmented Soybean multispectral imagery) is our contribution as a new tool for soybean high throughput phenotyping from UAS-based multispectral imagery.

Future works will address the integration of the obtained phenotyping variables into agronomic models.

REFERENCES

- [1] Schirrmann, M., Giebel, A., Gleiniger, F., Pflanz, M., Lentschke, J., and Dammer, K. H. "Monitoring agronomic parameters of winter wheat crops with low-cost UAV imagery". *Remote Sensing*, 8(9), 706 (2016).
- [2] Haghghattalab, A., Pérez, L. G., Mondal, S., Singh, D., Schinstock, D., Rutkoski, J., ... and Poland, J. "Application of unmanned aerial systems for high throughput phenotyping of large wheat breeding nurseries". *Plant Methods*, 12(1), 35 (2016).
- [3] Sankaran, S., Khot, L. R., Espinoza, C. Z., Jarolmasjed, S., Sathuvalli, V. R., Vandemark, G. J., ... and Pavek, M. J. "Low-altitude, high-resolution aerial imaging systems for row and field crop phenotyping: A review". *European Journal of Agronomy*, 70, 112-123 (2015).
- [4] Chherawala, Y., Lepage, R., and Doyon, G. "Food grading/sorting based on color appearance through machine vision: The case of fresh cranberries". In *Information and Communication Technologies, 2006. ICTTA'06. 2nd (Vol. 1, pp. 1540-1545). IEEE (2016).*
- [5] Whalley, J. L., and Shanmuganathan, S. "Applications of image processing in viticulture: A review" (2013).

- [6] Houborg, R., and Boegh, E. "Mapping leaf chlorophyll and leaf area index using inverse and forward canopy reflectance modeling and SPOT reflectance data". *Remote sensing of environment*, 112(1), 186-202 (2008).
- [7] Caturegli, L., Corniglia, M., Gaetani, M., Grossi, N., Magni, S., Migliazzi, M., ... and Raffaelli, M. "Unmanned aerial vehicle to estimate nitrogen status of turfgrasses". *PLoS One*, 11(6), e0158268 (2016).
- [8] Schmidt, K. S., and Skidmore, A. K. "Spectral discrimination of vegetation types in a coastal wetland". *Remote sensing of Environment*, 85(1), 92-108 (2003).
- [9] Khan, S. H., Hayat, M., Bennamoun, M., Soheli, F. A., and Togneri, R. "Cost-sensitive learning of deep feature representations from imbalanced data". *IEEE transactions on neural networks and learning systems*, 29(8), 3573-3587 (2018).
- [10] Berni, J. A. J., Zarco-Tejada, P. J., Suárez, L., González-Dugo, V., and Fereres, E. "Remote sensing of vegetation from UAV platforms using lightweight multispectral and thermal imaging sensors". *Int. Arch. Photogramm. Remote Sens. Spatial Inform. Sci.*, 38(6) (2009).
- [11] Turner, D.; Lucieer, A.; Malenovsky, Z.; King, D.H., Robinson, S.A. "Spatial co-registration of ultra-high resolution visible, multispectral and thermal images acquired with a micro-UAV over Antarctic moss beds". *Remote Sensing*, 6, 4003–4024 (2014).
- [12] Remondino, F.; Fraser, C. "Digital camera calibration methods: Considerations and comparisons". *Int. Arch. Photogramm. Remote Sens. Spat. Inf. Sci.*, 36, 266–272 (2006).
- [13] Herrero-Huerta, M., González-Aguilera, D., Rodríguez-Gonzálvez, P. and Hernández-López, D. "Vineyard yield estimation by automatic 3D bunch modelling in field conditions". *Computers and electronics in agriculture*, 110, 17-26 (2015).
- [14] Strecha, C., Bronstein, A., Bronstein, M., and Fua, P. "LDAHash: Improved matching with smaller descriptors". *IEEE transactions on pattern analysis and machine intelligence*, 34(1), 66-78 (2012).
- [15] Herrero-Huerta, M., Hernández-López, D., Rodríguez-Gonzálvez, P., González-Aguilera, D. and González-Piqueras, J. "Vicarious radiometric calibration of a multispectral sensor from an aerial trike applied to precision agriculture". *Computers and Electronics in Agriculture*, 108, 28-38 (2014).
- [16] Open Source Computer Vision Library, <http://sourceforge.net/projects/opencvlibrary/> (accessed February 2019).
- [17] Hartigan, J. A., and Wong, M. A. "Algorithm AS 136: A k-means clustering algorithm". *Applied statistics*, 100-108 (1979).
- [18] Canny, J., A. "Computational Approach To Edge Detection". *IEEE Trans. Pattern Analysis and Machine Intelligence*, 8(6):679–698 (1986).
- [19] Weinmann, M., Jutzi, B., and Mallet, C. "Semantic 3D scene interpretation: a framework combining optimal neighborhood size selection with relevant features". *Ann. Photogramm. Remote Sens. Spat. Inf. Sci.* 2, 181–188. doi: 10.5194/isprsannals-II-3-181-2014 (2014).
- [20] Jolliffe, I. T. (ed.). "Graphical representation of data using principal components". *Principal Component Analysis* (New York, NY: Springer), 78–110 (2002).
- [21] Rouse, J.W.; Haas, R.H.; Schell, J.A.; Deering D.W. "Monitoring vegetation systems in the Great Plains with ERTS". In *Proceedings of the Third ERTS Symposium*, NASA: Washington, DC, USA; NASA SP-351; pp. 309–317 (1973).